© 2014. Published by The Company of Biologists Ltd | Development (2014) 141, 3859-3867 doi:10.1242/dev.114900

RESEARCH ARTICLE

Head formation: OTX2 regulates *Dkk1* and *Lhx1* activity in the anterior mesendoderm

Chi Kin Ip[1,2,*], Nicolas Fossat[1,2,*,‡], Vanessa Jones[1], Thomas Lamonerie[3] and Patrick P. L. Tam[1,2]

ABSTRACT

The *Otx2* gene encodes a paired-type homeobox transcription factor that is essential for the induction and the patterning of the anterior structures in the mouse embryo. *Otx2* knockout embryos fail to form a head. Whereas previous studies have shown that *Otx2* is required in the anterior visceral endoderm and the anterior neuroectoderm for head formation, its role in the anterior mesendoderm (AME) has not been assessed specifically. Here, we show that tissue-specific ablation of *Otx2* in the AME phenocopies the truncation of the embryonic head of the *Otx2* null mutant. Expression of *Dkk1* and *Lhx1*, two genes that are also essential for head formation, is disrupted in the AME of the conditional *Otx2*-deficient embryos. Consistent with the fact that *Dkk1* is a direct target of OTX2, we showed that OTX2 can interact with the H1 regulatory region of *Dkk1* to activate its expression. Cross-species comparative analysis, RT-qPCR, ChIP-qPCR and luciferase assays have revealed two conserved regions in the *Lhx1* locus to which OTX2 can bind to activate *Lhx1* expression. Abnormal development of the embryonic head in *Otx2;Lhx1* and *Otx2;Dkk1* compound mutant embryos highlights the functional intersection of *Otx2*, *Dkk1* and *Lhx1* in the AME for head formation.

KEY WORDS: Anterior mesendoderm, *Otx2*, *Dkk1*, *Lhx1*, Head formation, Mouse

INTRODUCTION

The gene *orthodenticle homologue 2* (*Otx2*) encodes a paired-type homeobox transcription factor that controls the expression of target genes by binding to regulatory regions containing the YTAATNN motifs (Kimura-Yoshida et al., 2005; Chatelain et al., 2006). In the mouse, *Otx2* is expressed in the inner cell mass of the blastocyst (at embryonic day E3.5) and in the visceral endoderm of the E5.5 pre-gastrulation embryo (Kimura et al., 2001). It is also initially widely expressed in the epiblast, but becomes progressively regionalised during gastrulation to an anterior domain of the ectoderm (anterior neuroectoderm, ANE) that contains the precursor cells of the prosencephalon and the mesencephalon of the embryonic brain (Tam, 1989; Ang et al., 1994; Cajal et al., 2012).

Loss of *Otx2* in the mouse impedes morphogenetic tissue movement in the pre-gastrulation embryo, arrests germ layer formation during gastrulation and disrupts the morphogenesis of the embryonic head (Acampora et al., 1995; Matsuo et al., 1995; Ang et al., 1996). In $Otx2^{-/-}$ mutants, the precursor cells for the anterior visceral endoderm (AVE) fail to translocate from the distal site to the anterior region of the pre-gastrulation stage embryo. The absence of the AVE causes the loss of the source of morphogenetic signals for inducing neural differentiation of the ANE (Kimura et al., 2000). Lineage-tracing experiments have shown that *Otx2* activity in the visceral endoderm is required for navigating the cell movement (Kimura et al., 2000; Perea-Gomez et al., 2001).

Among the signalling pathway factors that are expressed in the visceral endoderm (Pfister et al., 2007) is Dickkopf homologue 1 (DKK1), an antagonist of WNT signalling (Kemp et al., 2005; Lewis et al., 2007; Fossat et al., 2012) and a downstream target of OTX2 (Kimura-Yoshida et al., 2005). *Dkk1* expression in the visceral endoderm is abolished in the $Otx2^{-/-}$ embryos (Zakin et al., 2000; Perea-Gomez et al., 2001). In transgenic $Otx2^{Dkk1/Dkk1}$ embryos, expression of *Dkk1* from the *Otx2* locus can rescue the migration defects of *Otx2*-deficient visceral endoderm cells. Head development, however, is still defective, indicating that positioning of the visceral endoderm is insufficient to reconstitute the genetic or signalling activity required for head formation (Kimura-Yoshida et al., 2005). *Otx2* function can be substituted by another *Otx* gene, *Otx1*, or its fly homologue *otd*. Chimeric mice or $Otx2^{Otx1/Otx1}$ and $Otx2^{otd/otd}$ transgenic mice that respectively express *Otx2*, *Otx1* or *otd* only in the visceral endoderm display normal cell migration in the visceral endoderm and the induction of the ANE, but still fail to form a proper brain (Acampora et al., 1998, 2001; Rhinn et al., 1998). These findings suggest that *Otx2* function is required in other embryonic tissue besides the visceral endoderm for maintaining the differentiation potential of the ANE.

Chimera experiments have shown that OTX2 acts cell-autonomously to maintain the expression of the anterior neuronal markers *Hesx1*, *Wnt1*, *Cdh4* and *Efna2* in the ANE (Rhinn et al., 1999), whereas inactivating *Otx2* in epiblast stem cells impairs the differentiation of anterior neural tissues (Iwafuchi-Doi et al., 2012; Acampora et al., 2013). These results highlight the intrinsic requirement of *Otx2* activity in the ANE for differentiation. The layer of endoderm cells and the midline structure (the anterior mesendoderm, AME) that are associated with the ANE are both derived from the epiblast during gastrulation. The AME expresses signalling pathway genes and its integrity is essential for the development of the anterior neural structures (Camus et al., 2000; Hallonet et al., 2002; Robb and Tam, 2004; Pfister et al., 2007). *Otx2* is also expressed in the AME but its tissue-specific function in the induction or maintenance of the ANE has not been tested directly.

In the present study, we have examined the requirement of *Otx2* in the AME by Cre-mediated ablation of the gene activity in *Otx2* AME-conditional knockout (*Otx2*-ameCKO) mutant embryos. Our results show that *Otx2* is required in the AME for the induction of anterior neural tissues and head formation. Loss of *Otx2* in the

[1]Embryology Unit, Children's Medical Research Institute, Locked Bag 23, Wentworthville, New South Wales 2145, Australia. [2]Discipline of Medicine, Sydney Medical School, University of Sydney, New South Wales 2006, Australia. [3]Equipe Neurodéveloppement, Institut de Biologie Valrose, UMR UNS/CNRS 7277/INSERM 1091, Université Nice Sophia Antipolis, Parc Valrose, 06108 Nice cedex 2, France.
*These authors contributed equally to this work

‡Author for correspondence (nfossat@cmri.org.au)

Received 29 June 2014; Accepted 10 August 2014

Development (2014) 141, 3859-3867 doi:10.1242/dev.114900

AME is accompanied by the downregulation of *Dkk1* and *Lhx1*. Results of RT-qPCR, ChIP-qPCR and luciferase assays indicate that these two genes are likely to be direct transcriptional targets of OTX2 in the AME. The analysis of compound mutant embryos shows that they both act synergistically with *Otx2* in this structure for head formation.

RESULTS

Otx2 is required in the AME for head formation

To analyse the specific requirement of *Otx2* in the AME, we used the *Foxa2-mcm* mouse line that expresses tamoxifen-inducible *MerCreMer* recombinase [*Foxa2*$^{tm2(Cre/Esr1*)Moon}$ – Mouse Genome Informatics] in *Foxa2*-expressing AME (Park et al., 2008). The expression pattern of R26R Cre-reporter (Soriano, 1999) in *Foxa2*$^{+/mcm}$;*Rosa26*$^{+/R26R}$ embryos treated with tamoxifen at E6.5 and harvested 30 h later revealed the presence of X-Gal-stained cells in the endoderm layer, predominantly in the anterior definitive endoderm and the axial AME (Fig. 1A). *Otx2*$^{flox/flox}$;*Foxa2*$^{mcm/mcm}$ mice were crossed with *Otx2*$^{+/-}$ mice to produce *Otx2*$^{+/flox}$;*Foxa2*$^{+/mcm}$ and *Otx2*$^{flox/-}$;*Foxa2*$^{+/mcm}$ embryos. These embryos were treated with tamoxifen or mock vehicle once at E6.5 and collected 30 h after treatment. Histology of the embryo showed that *Otx2* expression was reduced in the midline tissue of the tamoxifen-treated *Otx2*$^{flox/-}$;*Foxa2*$^{+/mcm}$ embryos (the *Otx2*-ameCKO embryos) compared with vehicle-treated (mock control) *Otx2*$^{flox/-}$;*Foxa2*$^{+/mcm}$ embryos (Fig. 1B). In addition, the epithelial cells in the midline of the *Otx2*-ameCKO embryo were shorter than the columnar AME cells of the control embryo (Fig. 1B).

Whereas *Foxa2-mcm* activity was widely expressed in the endoderm and the AME in the anterior region of the embryo after tamoxifen treatment at E6.5 (Fig. 1A), the impact of the ablation of *Otx2* is likely to be limited to the AME, based on the following considerations: (a) *Otx2* expression is confined to the tissues close to the midline, i.e. the AME and the immediately adjacent endoderm cells, thus suggesting that the ablation of *Otx2* in the non-expressing cells would not have any impact on the phenotype; (b) the descendants of the AVE that are present in the E6.5 embryo at the time of tamoxifen treatment are mostly found in the extraembryonic yolk sac (Thomas and Beddington, 1996; Shimono and Behringer, 2003). That practically no *lacZ*-positive cells were present in the yolk sac endoderm of the

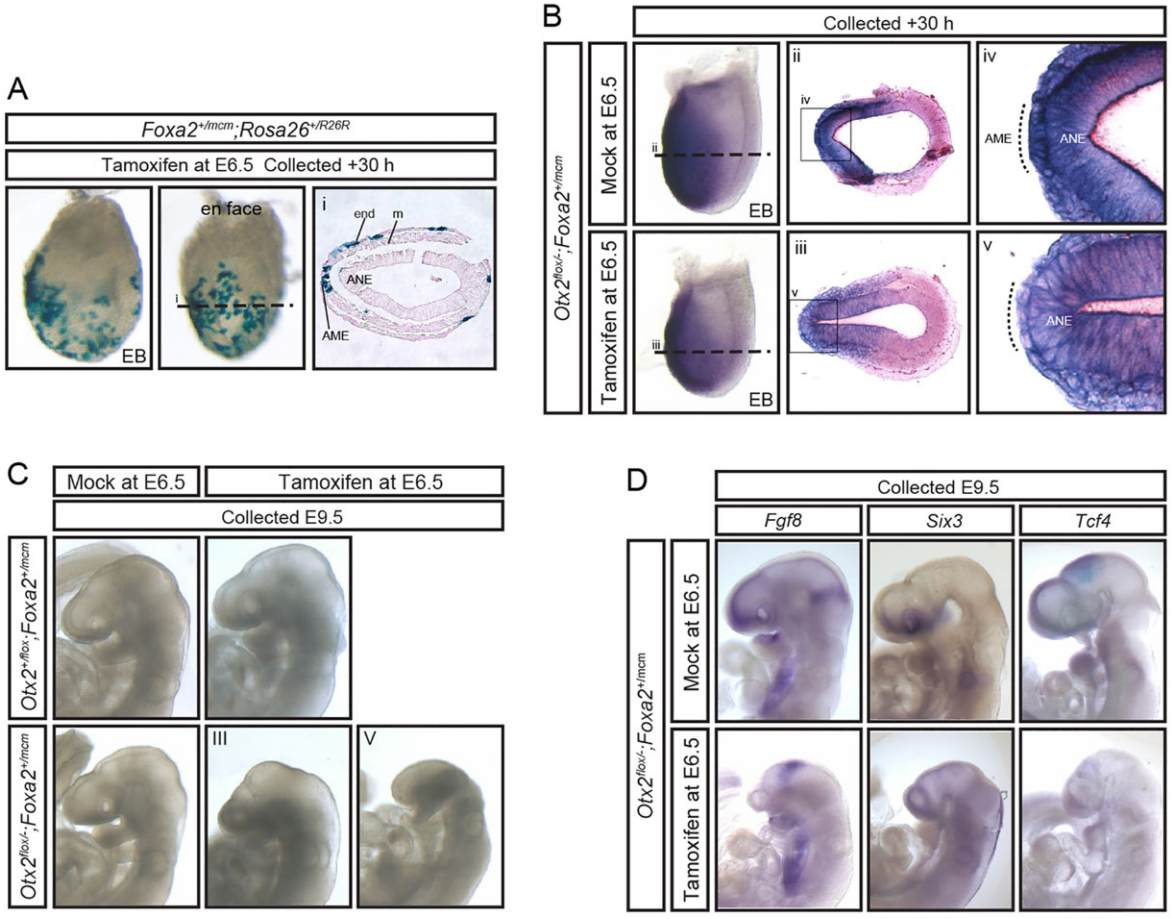

Fig. 1. *Otx2* ablation in the AME results in head truncation. (A) X-Gal staining of early bud (EB) stage *Foxa2*$^{+/mcm}$;*Rosa26*$^{+/R26R}$ embryos collected 30±2 h after tamoxifen injection at E6.5. Plan of section (i) is indicated by the dashed line in centre image. (B) *Otx2* expression of EB stage *Otx2*$^{flox/-}$;*Foxa2*$^{+/mcm}$ embryos collected 30±2 h after injection of tamoxifen or vehicle only (mock) at E6.5. Plan of section (ii and iii) is indicated by the straight dashed line in images on the left hand. Images (iv) and (v) correspond to the boxed areas in (ii) and (iii), respectively. The AME of mock embryo and the midline tissue of the tamoxifen-treated embryo are marked by curved dashed lines. (C) E9.5 *Otx2*$^{+/flox}$;*Foxa2*$^{+/mcm}$ and *Otx2*$^{flox/-}$;*Foxa2*$^{+/mcm}$ embryos after tamoxifen or mock injection at E6.5. Category of the head phenotype is indicated. (D) Expression of telencephalon markers *Fgf8* and *Six3*, diencephalon marker *Tcf4* and midbrain-hindbrain junction marker *Fgf8* in E9.5 mock- and tamoxifen-treated *Otx2*$^{flox/-}$;*Foxa2*$^{+/mcm}$ embryos. AME, anterior mesendoderm; ANE, anterior neurectoderm; end, endoderm; m, mesoderm. Lateral view of whole-mount specimens and anterior side to the left, except for *en face* view.

Development (2014) 141, 3859-3867 doi:10.1242/dev.114900

Table 1. Frequency of abnormal head phenotype of E9.5 embryos generated in crosses between *Otx2*$^{flox/flox}$;*Foxa2*$^{mcm/mcm}$ and *Otx2*$^{+/-}$ mice

	Number of embryos per head phenotype category					Number of embryos analysed (% with head defect)
Phenotype category	I	II	III	IV	V	
Genotype						
Otx2$^{flox/-}$;*Foxa2*$^{+/mcm}$ (Mock)	6	1	0	0	0	7 (14%)
Otx2$^{flox/-}$;*Foxa2*$^{+/mcm}$ (Tamoxifen)	0	1	4	4	1	10 (100%)

$P<0.01$ ($\chi^2=14.93$) after χ^2 test for the distribution of embryos across the phenotype categories between the two conditions of injection.
Note: number of embryos of the following genotypes showing phenotype class II (the only class observed)/total number of embryos of following genotypes: *Otx2*$^{+/flox}$;*Foxa2*$^{+/mcm}$ oil (0/8), tamoxifen (1/7).

Foxa2$^{+/mcm}$;*Rosa26*$^{+/R26R}$ embryos treated with tamoxifen at E6.5 (Fig. 1A) suggests that the Cre activity was not activated in the AVE, which should still harbour an undeleted *Otx2*^{flox} allele. However, our results do not exclude the possibility that some AVE descendants in the anterior endoderm (Kwon et al., 2008) contain a Cre-mediated ablation of the *Otx2* gene. Nevertheless, it is likely that the presence of a small subset of *Otx2*-deficient AVE descendants (given the mosaic pattern of Cre activity) has no significant functional consequences that contribute to the mutant phenotype.

At E9.5, the *Otx2*-ameCKO embryos displayed a fully penetrant head truncation phenotype (in a range between category II and V; see Materials and Methods) (Table 1; Fig. 1C). Fourteen percent of mock control *Otx2*$^{flox/-}$;*Foxa2*$^{+/mcm}$ embryos showed a mild truncation phenotype (category II) (Table 1) that is reminiscent of the hypomorphic heterozygous *Otx2*$^{+/-}$ embryo (Acampora et al., 1995; Fossat et al., 2006). A similar frequency of mild truncation (category II) was found in the tamoxifen-treated *Otx2*$^{+/flox}$;*Foxa2*$^{+/mcm}$ embryos but not in the mock control with the same genotype (Table 1). Analysis of molecular markers revealed a reduced dorsal and ventral rostral telencephalon (*Fgf8*, *Six3*) and dorsal diencephalon (*Tcf4*) in the *Otx2*-ameCKO embryos (Fig. 1D). *Otx2* activity in the AME is therefore essential for head formation.

Loss of *Otx2* impacts on *Dkk1* and *Lhx1* expression

In the *Otx2*-ameCKO embryos, *Shh*-expressing cells were present in the anterior midline that resembled the AME of the mock control embryo (Fig. 2A), indicating that the loss of *Otx2* in the *Foxa2*-expressing tissue does not affect AME formation. Given that *Dkk1* is a known target of OTX2 (Kimura-Yoshida et al., 2005) and that it is required in the AME for head development (Mukhopadhyay et al., 2001; Lewis et al., 2007), we examined *Dkk1* expression in the *Otx2*-ameCKO embryos and observed that its expression was reduced in the AME of these mutants (Fig. 2B).

Loss of *Lhx1*, which encodes the LIM-homeobox 1 transcription factor, also leads to severe head truncation (Shawlot and Behringer, 1995). *Lhx1* is required in both the visceral endoderm and the epiblast for head formation. Chimeric embryos that have lost *Lhx1* activity in the visceral endoderm or the epiblast phenocopy the head truncation of the *Otx2*-ameCKO embryos (Shawlot et al., 1999). Consistent with a contribution by *Lhx1* to the genesis of the mutant phenotype, *Lhx1* expression was downregulated in the midline cells in the endoderm layer, but not in the definitive endoderm or the mesoderm of the *Otx2*-ameCKO embryo (Fig. 2B). These results suggest that the reduction or loss of *Lhx1* and *Dkk1* activity in the AME underpins the impact of loss of *Otx2* function on forebrain and head formation.

OTX2 activates *Dkk1* and *Lhx1* expression

To investigate whether OTX2 can regulate *Dkk1* and *Lhx1*, their expression was assessed in mouse P19 embryonal carcinoma cells transfected with plasmid expressing wild-type OTX2 or a mutant form of OTX2 (hereafter referred to as OTX2-3pm) that is unable to bind DNA due to three mismatch point mutations in the homeodomain coding sequence (Chatelain et al., 2006). Both the wild type and the variant form of OTX2 were tagged with GFP and were expressed in the nucleus (Fig. 3A), as previously reported (Chatelain et al., 2006). In the transfected P19 cells, *Dkk1* and *Lhx1* expression were upregulated by OTX2 but not by OTX2-3pm (Fig. 3B). These results show that OTX2 can activate *Lhx1* and *Dkk1* expression and that this is dependent on the ability of OTX2 to bind DNA.

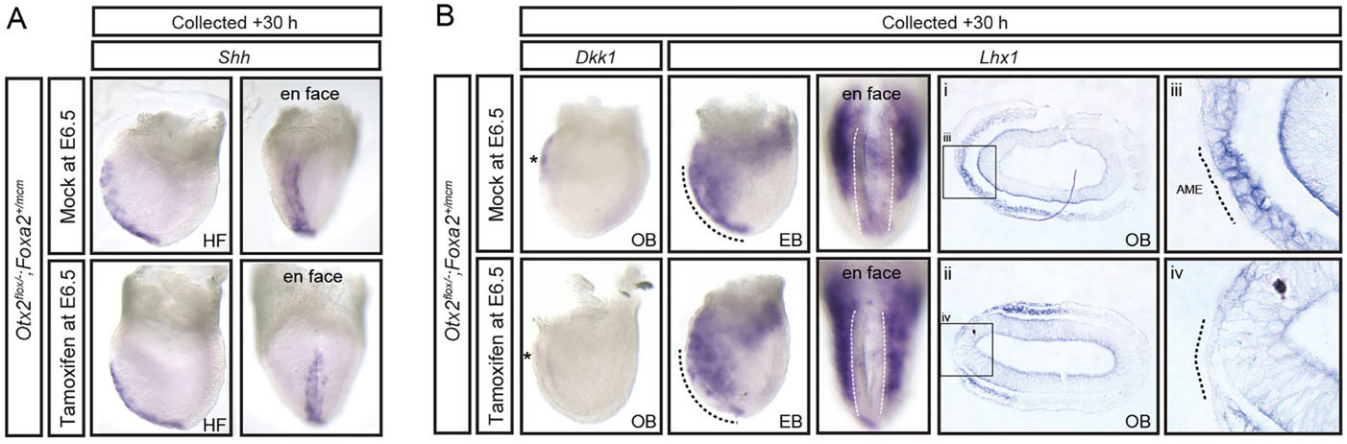

Fig. 2. *Lhx1* and *Dkk1* expression is impaired in the AME of *Otx2*-ameCKO embryos. (A) Expression of *Shh* in the anterior midline tissues of headfold (HF) stage *Otx2*$^{flox/-}$;*Foxa2*$^{+/mcm}$ embryos collected 30±2 h after tamoxifen or mock treatment at E6.5. (B) *Dkk1* and *Lhx1* expression in no-bud (OB) and EB stage mock- and tamoxifen-treated *Otx2*$^{flox/-}$;*Foxa2*$^{+/mcm}$ embryos collected 30±2 h after treatment at E6.5. Images (iii) and (iv) correspond to boxed areas in (i) and (ii), respectively. *Dkk1* expression in AME of mock-treated embryos and the corresponding area in tamoxifen-treated embryos is marked by an asterisk. *Lhx1* expression in AME of mock-treated embryos and the corresponding area in tamoxifen-treated embryos is marked by a black dashed line (lateral view and section) or delineated by a white dashed line (*en face* view). Lateral view of whole-mount specimens and anterior side to the left, except for *en face* view.

Development (2014) 141, 3859-3867 doi:10.1242/dev.114900

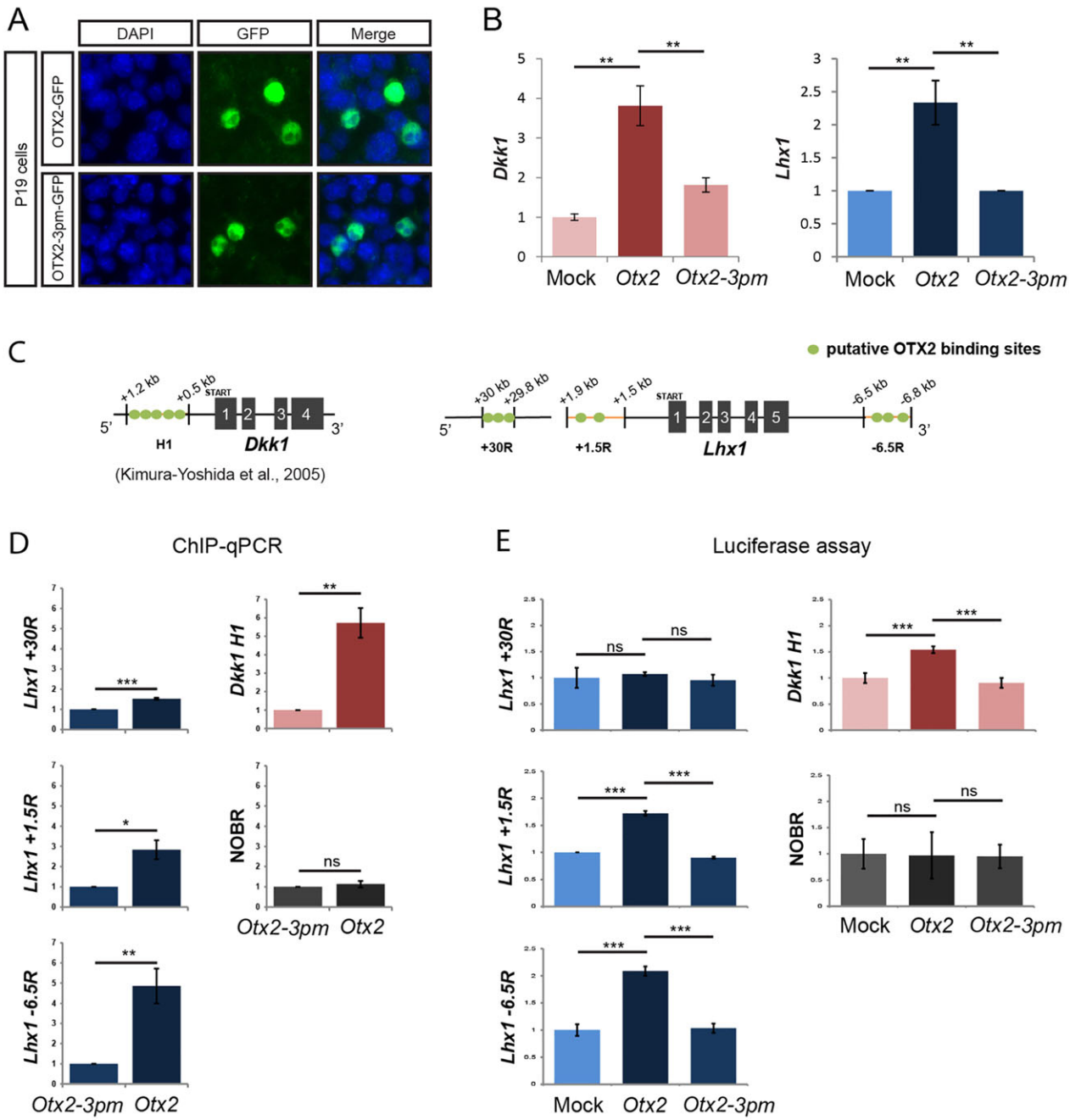

Fig. 3. OTX2 binds and activates *Dkk1* and *Lhx1*. (A) OTX2-GFP, OTX2-3pm-GFP and nuclei (DAPI staining) visualised in P19 cells transfected with a pCMV-*Otx2-gfp* or a pCMV-*Otx2-3pm-gfp* expression vector. (B) Real-time RT-PCR quantitation of *Dkk1* and *Lhx1* expression relative to *β-actin* expression in P19 cells transfected with pCMV-*gfp* (mock), pCMV-*Otx2-gfp* or pCMV-*Otx2-3pm-gfp* expression vector. (C) Schematic representation (not to scale) of *Dkk1* and *Lhx1* loci. Coordinates are indicated relative to the START codon. Grey boxes, exons; orange lines, conserved regulatory regions; green circles, putative OTX2-binding sites. (D) Real-time PCR quantitation of indicated *Lhx1* and *Dkk1* regions or a region without OTX2-binding motifs (NOBR) immunoprecipitated with an anti-GFP antibody from P19 cells transfected with pCMV-*Otx2-gfp* or pCMV-*Otx2-3pm-gfp* expression vector. Results are normalised to real-time PCR quantitation performed from input samples. (E) Firefly luciferase activity quantification relative to Renilla luciferase activity in 3T3 cells transfected with the firefly luciferase construct harbouring the region indicated, a Renilla luciferase expression vector and pCMV-*gfp* (mock), pCMV-*Otx2-gfp* or pCMV-*Otx2-3pm-gfp* expression vector. Three independent transfections were performed for each RT-qPCR, ChIP-qPCR and luciferase assay. Each histogram represents the mean±s.e.m. of triplicate analysis for each transfection. *P*-value <0.05 (*), <0.01 (**), <0.001 (***), >0.05 (ns, non-significant) by *t*-test.

OTX2 binds to regulatory elements to activate *Dkk1* and *Lhx1*

OTX2 protein binds YTAATNN motifs (Kimura-Yoshida et al., 2005; Chatelain et al., 2006) and is known to directly control *Dkk1* expression by binding the H1 regulatory region located ∼500 bp upstream of the *Dkk1* START codon (Kimura-Yoshida et al., 2005). No OTX2 regulatory regions have been reported for the *Lhx1* locus. We therefore performed a multi-species comparative analysis to search for conserved regions containing at least one OTX2-binding motif and located within 50 kb upstream and 15 kb downstream of the START codon of *Lhx1*. Three such regions were found: two located 30 kb (+30R) and 1.5 kb (+1.5R) upstream, and one located 6.5 kb

Development (2014) 141, 3859-3867 doi:10.1242/dev.114900

(−6.5R) downstream of the START codon (supplementary material Figs S1-S3). The binding of OTX2 to these regions was tested by chromatin immunoprecipitation (ChIP)-qPCR experiments using an anti-GFP antibody and P19 cells expressing *Otx2-gfp* or *Otx2-3pm-gfp*. +1.5R and −6.5R regions were significantly enriched in chromatin precipitated with OTX2 when compared with chromatin precipitated with OTX2-3pm (Fig. 3D). The same was observed for the +30R region, although the binding appeared to be weaker. We could also confirm the binding of OTX2 to the H1 region of *Dkk1*. No enrichment was observed for a region of the genome that has no OTX2-binding motif (NOBR).

We tested whether these conserved regions could act as enhancers to mediate the activation of gene expression by OTX2. These sequences were cloned into a reporter plasmid that carries a minimal promoter and a gene encoding the firefly luciferase protein. Elevated firefly luciferase activity (compared with the mock control) was detected when co-transfected with an *Otx2* expression vector and the reporter plasmid containing the *Dkk1* H1 region, and with the *Lhx1* +1.5R and −6.5R regions, but not with the *Lhx1* +30R region or the DNA fragment without OTX2-binding motif (NOBR) (Fig. 3E). Luciferase activity was not different from the mock control when P19 cells were co-transfected with an *Otx2-3pm* expression vector (Fig. 3E). These results show that both the *Dkk1* H1 region and the *Lhx1* +1.5R and −6.5R regions are bound by OTX2 to activate gene expression. Interestingly, ChIP-sequencing data of the ENCODE project support the notion that regions equivalent to +1.5R and −6.5R regions in human *LHX1* are regulatory (Wang et al., 2012).

Synergistic interaction of *Otx2* with *Lhx1* and *Dkk1* in head formation

Loss of *Otx2* produces a phenocopy of the *Lhx1*-null and *Dkk1*-null head truncation phenotype (Acampora et al., 1995; Matsuo et al., 1995; Shawlot and Behringer, 1995; Ang et al., 1996; Mukhopadhyay et al., 2001). *Otx2*, *Lhx1* and *Dkk1* display overlapping domain of expression in the AME during gastrulation (Fig. 4A). The downregulation of *Lhx1* and *Dkk1* in the AME of *Otx2*-ameCKO embryos raised the possibility that *Otx2* acts synergistically with *Lhx1* and *Dkk1* in facilitating head development. We tested this hypothesis by analysing the phenotype of AME-specific compound *Otx2;Lhx1* and *Otx2;Dkk1* heterozygous mutant embryos. This was accomplished by generating $Otx2^{+/flox};Lhx1^{+/-};Foxa2^{+/mcm}$

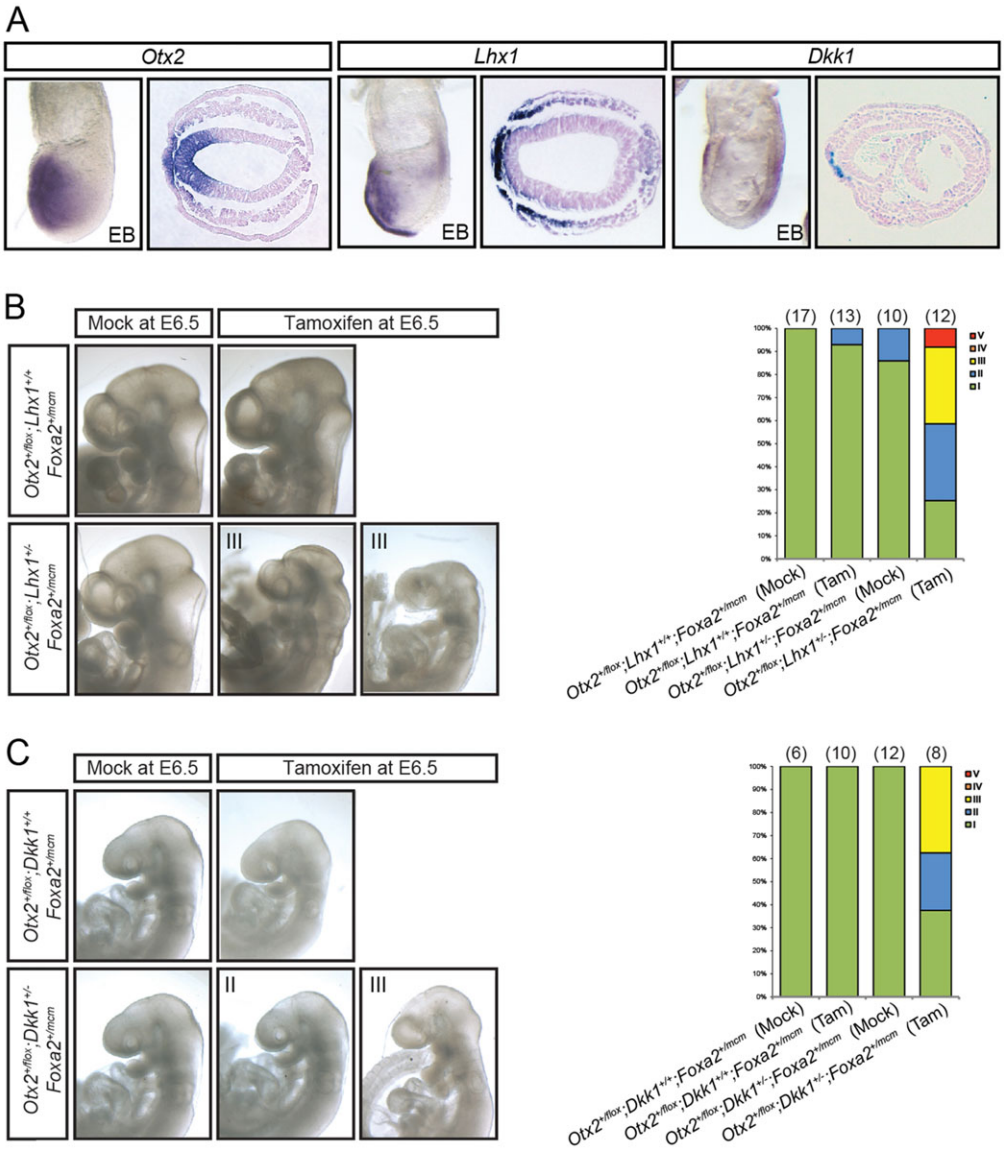

Fig. 4. Synergistic interaction of *Otx2* and *Lhx1* or *Dkk1* in the AME for head formation. (A) Expression pattern of *Otx2*, *Lhx1* and *Dkk1* in EB mouse embryos. Right panels: transversal sections. (B) E9.5 $Otx2^{+/flox};Lhx1^{+/-};Foxa2^{+/mcm}$ and $Otx2^{+/flox};Lhx1^{+/+};Foxa2^{+/mcm}$ embryos after tamoxifen or mock injection at E6.5. (C) E9.5 $Otx2^{+/flox};Dkk1^{+/-};Foxa2^{+/mcm}$ and $Otx2^{+/flox};Dkk1^{+/+};Foxa2^{+/mcm}$ embryos after tamoxifen or mock injection at E6.5. Category of the head phenotype is indicated. The distribution of embryos of different genotypes to the five head phenotype categories is presented in histograms on the right. The length of the bars indicates the percentage of embryos in each phenotype category. The number of embryos scored for each genotype is given in parentheses. Lateral view of whole-mount specimen and sections with anterior side to the left.

Development (2014) 141, 3859-3867 doi:10.1242/dev.114900

(compound *Otx2;Lhx1*) and *Otx2*$^{+/flox}$;*Dkk1*$^{+/-}$;*Foxa2*$^{+/mcm}$ (compound *Otx2;Dkk1*) mutant embryos from a cross between *Otx2*$^{flox/flox}$;*Foxa2*$^{mcm/mcm}$ and *Lhx1*$^{+/-}$ mice or *Dkk1*$^{+/-}$ mice, respectively. Induction of MerCreMer recombinase was achieved by tamoxifen administration at E6.5, as for the *Otx2*-ameCKO embryos. The AME of these mutant embryos were populated by *Otx2*$^{+/-}$;*Lhx1*$^{+/-}$ cells (in compound *Otx2;Lhx1* mutants) or by *Otx2*$^{+/-}$;*Dkk1*$^{+/-}$ cells (in compound *Otx2;Dkk1* mutants). In the compound *Otx2;Lhx1* embryos, the mutants displayed more severe head truncation at a higher frequency than mutant embryos with mock injection (Fig. 4B; Table 2), as well as *Otx2*$^{+/flox}$;*Lhx1*$^{+/+}$;*Foxa2*$^{+/mcm}$ embryos generated from the same cross (tamoxifen- and mock-injected; Fig. 4B; Table 2). Similarly, the compound *Otx2;Dkk1* embryos also displayed a more severe truncated head phenotype at a higher frequency than mutant embryos with mock injection or tamoxifen- and mock-treated *Otx2*$^{+/flox}$;*Dkk1*$^{+/+}$;*Foxa2*$^{+/mcm}$ embryos (Fig. 4C; Table 3). Taken together, these results show that *Otx2* acts synergistically with *Lhx1* and *Dkk1* specifically in the AME for head formation.

DISCUSSION

Results of this study have highlighted a crucial role for *Otx2* in the AME in promoting head and forebrain formation, and that OTX2 function might be mediated by regulating the activity of two downstream genes, *Lhx1* and *Dkk1*, that are also essential for head morphogenesis. These two genes are likely to be the transcriptional targets of OTX2 that activates their expression by binding conserved enhancer regions.

Otx2 is expressed at multiple sites in the early embryo, such as the visceral endoderm, the epiblast and the epiblast-derived ANE and AME, and might have tissue-specific functions at these sites during the formation of the head primordium (Ang et al., 1994; Kimura et al., 2000). In the visceral endoderm of the pre-gastrulation stage embryo, *Otx2* is required for navigating the movement of cells towards the prospective anterior region (Acampora et al., 1998, 2001; Rhinn et al., 1998; Kimura et al., 2000; Perea-Gomez et al., 2001). The directional translocation of cells is instrumental for the establishment of the AVE. Loss of *Otx2* function impedes the movement of the visceral endoderm, which can be overcome by expressing *Dkk1* from the mutant *Otx2* locus (Kimura-Yoshida et al., 2005). Restoring the AVE through enhancing *Dkk1* activity in the visceral endoderm, however, does not rescue the *Otx2*-deficient embryo from developing head truncation defects. In a similar context, chimeric embryos comprising *Otx2*-expressing visceral endoderm and *Otx2*-deficient epiblast (Rhinn et al., 1998), and conditional mutant embryos with *Otx2* knocked out in *Otx2*-expressing epiblast-derivatives by inducible *Otx2*-CreER^{T2} activity (Fossat et al., 2006) also develop head truncation defects. By regulating expression of homeobox and cell adhesion genes *Otx2* has both cell-autonomous and non-autonomous functions in the ANE. Chimera embryos containing both *Otx2* mutant and wild-type cells in the ANE show reduced *Hesx1*, *Wnt1*, *Cdh4* and *Efna2* expression in mutant cells, which eventually enter into apoptosis (Rhinn et al., 1999). *Otx2* is also required for the dorso-ventral patterning of the brain (Puelles et al., 2003) and to delineate the mid-hindbrain boundary by antagonising *Gbx2*-expressing cells (Li and Joyner, 2001; Martinez-Barbera et al., 2001). These findings therefore indicate a separate requirement of *Otx2* activity in the epiblast and its derivatives, probably for the induction and maintenance of the neural potency of the anterior ectoderm and for brain morphogenesis. However, it is not known in which epiblast tissue compartment *Otx2* plays an essential role in the early phase of head development.

By targeting the ablation of *Otx2* to the *Foxa2*-expressing cells in the gastrula-stage embryo, *Otx2* expression has been specifically eliminated in the AME. The conditional mutant *Otx2*-ameCKO embryos display head truncation defect, principally a reduced forebrain and loss of the facial primordia, although not as severe as the complete truncation at the mid-hindbrain junction of the *Otx2*-null embryo (Acampora et al., 1995; Matsuo et al., 1995; Ang et al., 1996). The manifestation of a mutant phenotype is not due to the failure to form the anterior axial mesendoderm, but is associated with impaired morphogenetic activity, which is revealed by the downregulation of genes with key roles in head formation. *Otx2* is therefore required in a multi-phasic manner, first in the extraembryonic tissue for establishing the signalling source for tissue patterning, and later in the epiblast-derived tissues, where it plays a role in the AME for the maintenance of the anterior characteristics of the overlying ectoderm (this study), and its activity in the ANE drives the differentiation of the anterior neural progenitors.

The *Lhx1* gene that is downregulated in the AME of the *Otx2*-ameCKO embryo is similarly important for head formation and also displays several modes of functional requirement in head development. Loss of *Lhx1* leads to severe head truncation as in the *Otx2*-null mutant (Shawlot and Behringer, 1995). *Lhx1*-null embryos display abnormal shape due to disruption in germ layer morphogenesis and fail to form a proper head (Shawlot and Behringer, 1995; Shawlot et al., 1999). In the visceral endoderm, *Lhx1* is required to maintain angiomotin activity for the movement of the AVE at the onset of gastrulation (Shimono and Behringer, 1999, 2003). *Lhx1* is also required in epiblast-derived tissues for

Table 2. Frequency of abnormal head phenotype of embryos generated in crosses between *Otx2*$^{flox/flox}$;*Foxa2*$^{mcm/mcm}$ and *Lhx1*$^{+/-}$ mice

	Number of embryos per head phenotype category					Number of embryos analysed (% with head defect)
Phenotype category	I	II	III	IV	V	
Genotype						
Otx2$^{+/flox}$;*Lhx1*$^{+/-}$;*Foxa2*$^{+/mcm}$ (Mock)	9	1	0	0	0	10 (10%)
Otx2$^{+/flox}$;*Lhx1*$^{+/-}$;*Foxa2*$^{+/mcm}$ (Tamoxifen)	3	4	4	0	1	12 (75%)

P<0.05 (χ^2=9.69) after χ^2 test for the distribution of the embryos across the phenotype categories between the two conditions of injection.
Note: number of embryos of the following genotypes showing phenotype class II (the only class observed)/total number of embryos of following genotypes: *Otx2*$^{+/flox}$;*Lhx1*$^{+/+}$;*Foxa2*$^{+/mcm}$ oil (0/17), tamoxifen (1/13).

Table 3. Frequency of abnormal head phenotype of embryos generated in crosses between *Otx2*$^{flox/flox}$;*Foxa2*$^{mcm/mcm}$ and *Dkk1*$^{+/-}$ mice

	Number of embryos per head phenotype category					Number of embryos analysed (% with head defect)
Phenotype category	I	II	III	IV	V	
Genotype						
Otx2$^{+/flox}$;*Dkk1*$^{+/-}$;*Foxa2*$^{+/mcm}$ (Mock)	12	0	0	0	0	12 (0%)
Otx2$^{+/flox}$;*Dkk1*$^{+/-}$;*Foxa2*$^{+/mcm}$ (Tamoxifen)	3	2	3	0	0	8 (62.5%)

P<0.01 (χ^2=10) after χ^2 test for the distribution of the embryos across the phenotype categories between the two conditions of injection.
Note: none of the *Otx2*$^{+/flox}$;*Dkk1*$^{+/+}$;*Foxa2*$^{+/mcm}$ oil (n=6), tamoxifen (n=10) embryos showed head defects.

Development (2014) 141, 3859-3867 doi:10.1242/dev.114900

head formation (Shawlot et al., 1999). Both the chimeric embryo with *Lhx1*-active visceral endoderm and *Lhx1*-deficient epiblast, and the conditional mutant embryo with no *Lhx1* activity in the epiblast-derived tissues develop head truncation defects (Shawlot et al., 1999; Kwan and Behringer, 2002; Tanaka et al., 2010). In the present study, the synergistic effect of the combined loss of function of *Otx2* and *Lhx1* on the manifestation of the head phenotype and the effector-target relationship of *Otx2* and *Lhx1* are consistent with their co-requirement for head formation. Our results suggest that both gene products might be required in the AME for head formation, namely OTX2 by activating *Lhx1* expression and LHX1 by controlling target genes crucial for head formation that still need to be identified.

Some clues of the *Otx2* downstream activity that might have a role in head formation can be obtained from the study of its other target, *Dkk1*. DKK1 is a secreted molecule that inhibits WNT signalling for head formation (Fossat et al., 2012). Genetic experiments in mice demonstrated that an elevated level of WNT signalling activity impairs anterior development and that the increase in WNT signalling and the impairment are exacerbated by the absence of *Dkk1* (Fossat et al., 2011, 2012; Arkell and Tam, 2012; Arkell et al., 2013). The AVE is a source of secreted antagonists (*Dkk1*, *Sfrp1*, *Sfrp5* and *Cer1*) for modulating WNT signalling. However, lacking *Dkk1* activity only in the visceral endoderm has no impact on head formation (Mukhopadhyay et al., 2001). In the gastrulating embryo, *Dkk1* expression is restricted to the AME and the head truncation phenotype of $Dkk1^{-/-}$ embryos is likely to be due to the absence of *Dkk1* in this structure (Mukhopadhyay et al., 2001). *Dkk1* is a target of OTX2 in the AVE (Kimura-Yoshida et al., 2005). Here, we demonstrate that conditional ablation of *Otx2* in the AME leads to the downregulation of *Dkk1*, which also supports a direct regulation of *Dkk1* expression by OTX2 in the AME. Furthermore, we show a synergistic interaction between *Otx2* and *Dkk1* in the AME. OTX2 might therefore function through the regulation of *Dkk1* expression in the AME to modulate the level of WNT signalling perceived by the ANE during the development of the anterior neural structures.

Our study has therefore revealed a functional hierarchy of *Otx2-Dkk1* activity in the AME and that one function of *Otx2* is likely to be modulating the level of canonical WNT signalling activity for neural induction and the morphogenesis of the head. Whereas our findings have also established an *Otx2-Lhx1* transcriptional regulatory relationship, the downstream activity of the *Otx2-Lhx1* interaction in controlling head formation is presently unknown and awaits further investigation.

MATERIALS AND METHODS

Mouse strains, genotyping and crosses

$Otx2^{flox/flox}$ and $Otx2^{+/-}$ mice (Fossat et al., 2006), $Foxa2^{mcm/mcm}$ mice (Park et al., 2008), $Lhx1^{+/-}$ mice (Kwan and Behringer, 2002), $Dkk1^{+/-}$ mice (Mukhopadhyay et al., 2001) and $Rosa26^{+/R26R}$ mice (Soriano, 1999) were used for the genetic experiments in this study. Genotyping by PCR followed established protocols and was performed on DNA extracted from tail tissues of newborn mice or the yolk sac of embryos. The breeding strategies for the production of compound mutants as well as the number of embryos of each genotype that were analysed for head defects are described in Tables 1–3. All animal experimentation was approved by the Animal Ethics Committee of the Children's Medical Research Institute and of the Children's Hospital at Westmead, Sydney, Australia.

Embryo collection, staging and tamoxifen injection

Embryos were collected from gravid mice at the required gestational age or at specific time points after tamoxifen or mock treatment. Tamoxifen (Sigma-Aldrich) diluted at 10 mg/ml in canola oil was administered to gravid females by intraperitoneal injection at 100 µl (1 mg) per 20 g of body weight (the day of vaginal plug was taken as E0.5). For mock control, the same volume of canola oil without tamoxifen was administered. Embryos were staged according to criteria established by Downs and Davies (1993) or by somite number.

Analysis of mutant phenotypes and categorisation based on head defect

The morphology of mutant embryos was compared with stage-matched control embryos with specific attention to the size, the number of somites and the morphology of the head. The degree of head truncation was determined by measuring the head size, which was expressed as a ratio of the length of the dorsal margin of the silhouette of the head from the junction of the maxillary prominence and the base of the first branchial arch to the anterior border of the otic vesicles to the diameter of the otic vesicle (for a description of the normalisation of the measurement to account for the developmental status of the embryo see Lewis et al., 2007). Embryos were assigned to one of five categories based on the size of the fore- and midbrain: [I] Normal size (0% reduction), [II] ≤25% reduction, [III] 26-75% reduction, [IV] >75% reduction, [V] complete absence. As an example, the head size of class I embryos (normal size) was 15.37±0.42 units (n=6), compared with that of class II (the mildest reduction at ≤25%) size of 12.81±1.09 units (n=4), which is significantly different at P<0.0007 by two-tailed t-test.

In situ hybridisations, X-Gal staining and histology

In situ hybridisation and X-Gal staining were performed as previously described (Tam and Steiner, 1999; Fossat et al., 2007, 2011; Lewis et al., 2007). For histology analysis, embryos were embedded in paraffin, sectioned and counterstained with nuclear Fast Red and Eosin according to standard protocols (Tam and Steiner, 1999; Lewis et al., 2007). At least three specimens of each genotype were analysed for each marker tested.

Molecular cloning and plasmids

Expression vectors: pCMV-*GFP*, pCMV-*Otx2-GFP* and pCMV-*Otx2-3pm-GFP* plasmids have been described (Chatelain et al., 2006; Fossat et al., 2014).

Vectors for luciferase assay: regulatory elements were amplified by PCR from mouse genomic DNA with primers described below and cloned into the *Xho*I site or between the *Nhe*I and the *Kpn*I sites of the pGL3-promoter plasmid (Promega). The H1 region of *Dkk1* (Kimura-Yoshida et al., 2005) was amplified with 5′-ATCGCTCGAGCGAGGTTTGATTTGGGATCA-3′ and 5′-ATCGCTCGAGTATGAGTACCCTCGCTTTCT-3′ primers. The region 30 kb upstream of *Lhx1* ATG (+30R; 29,827-30,053 bp upstream of *Lhx1* START codon) was amplified with 5′-ATCGGCTAGCCCTG-TGCTCTCTTGTCCAT-3′ and 5′-ATCGGCTAGCAGGCCTGACATTT-CCAACAT-3′ primers. The region 1.5 kb upstream of *Lhx1* ATG (+1.5R; 1581-1877 bp upstream of *Lhx1* START codon) was amplified with 5′-ATCGGGTACCAAACAGACAGAAGGCGAGAT-3′ and 5′-ATCGG-CTAGCTCCGTTTCGGCATCAAGGA-3′ primers. The region 6.5 kb downstream of *Lhx1* ATG (−6.5R; 6591-6809 bp downstream of *Lhx1* START codon) was amplified with 5′-ATCGGGTACCGCTTGTGG-ATGTCAGATACT-3′ and 5′-ATCGGCTAGCTCTGGGGAACTTCAA-ACGTA-3′ primers. A region of the genome not bound by *Otx2* (NOBR; −1402 bp to −1660 bp downstream of *Hesx1* START codon) was amplified using 5′-ATCGGGTACCTTGGCTTCTCTTCCAGTTGT-3′ and 5′-ATCGGCTAGCCTGTATACACCTGTGAAGGT-3′ primers.

Cell transfection

Mouse embryonic carcinoma P19 cells and 3T3 fibroblasts were transfected using Fugene 6 (Roche) with pCMV-*GFP*, pCMV-*Otx2-GFP* or pCMV-*Otx2-3pm-GFP*. At 24 h after transfection, cells were washed and fixed for immunostaining or collected and snap-frozen for ChIP-qPCR experiments. For RT-qPCR analysis, at least 250,000 GFP-expressing cells were isolated by fluorescence-activated cell sorting (FACS) before being snap-frozen. For the luciferase assay, 3T3 cells were co-transfected with the pGL3-promoter constructs and with pRL Renilla luciferase control reporter vectors (Promega).

Development (2014) 141, 3859-3867 doi:10.1242/dev.114900

Immunostaining

Cells were washed with PBS, incubated for 5 min in 4% paraformaldehyde (PFA) with 0.5% Triton X-100, then for 20 min in 4% PFA at room temperature. After fixation, cells were washed with PBS, incubated for 15 min at room temperature with CAS-Block (Invitrogen), then for 40 min at 4°C with anti-GFP antibody (1:300; A11122, Invitrogen) diluted in CAS-Block. The following day, cells were washed with PBS and incubated for 40 min at room temperature with Alexa Fluor 488 anti-rabbit antibody (1:300) and 4′,6-diamidino-2-phenylindole (DAPI; Sigma-Aldrich; 1:1000) diluted in PBS. Cells were finally washed with PBS and embedded in Fluoromount-G (Invitrogen) for microscopy analysis.

RNA isolation, RT-PCR and qPCR

RNA from three independent transfections was extracted using an RNeasy Micro Kit (Qiagen). cDNA was synthesised from 100 ng RNA using the Superscript III First Strand System (Invitrogen). Quantitative PCR was performed in triplicate from 1:5 dilution of cDNA of each sample using the Rotorgene 6000 thermal cycler (Corbett Research), SYBR Green I (Molecular Probes) and Platinum Taq DNA Polymerase (Invitrogen). Primers used for assaying *β-actin* and *Dkk1* expression were previously described (Fossat et al., 2011). The primers 5′-AAGCAACTGGA-GACGTTGAA-3′ and 5′-CTAGCGCGCTTAGCTGTTT-3′ were used to assay *Lhx1* expression. PCR conditions (Fossat et al., 2011) were similar for all three genes.

Luciferase assay

Cells were collected from three independent transfections. The luciferase assay was performed using the Dual-Luciferase Reporter Assay System (Promega) according to the manufacturer's instructions. Firefly and Renilla luciferase activities were detected by a luminometer [Turner Designs TD-20/20 luminometer; dual-luciferase Renilla (DLR) mode; time-measurement delay 2 s; integrate time 6 s]. Relative firefly luciferase activity was measured and normalised relative to Renilla luciferase activity. Furthermore, all measurements were normalised to luciferase activity quantified from an experiment performed with a reporter vector without regulatory regions (pGL3-promoter).

ChIP-qPCR

Three million P19 cells were washed with PBS, dissociated with trypsin and centrifuged at 800 ***g*** for 5 min. The cell pellet was resuspended and rotated in 1 ml PBS with 1% formaldehyde for 10 min. Fixation was stopped by adding 0.15 M glycine. From this point on, the experiment was performed at 4°C. Cells were washed three times with ice-cold PBS and centrifuged at 800 ***g*** for 10 min. The cell pellet was resuspended and incubated for 10 min in 1 ml LB-A buffer [50 mM Hepes-KOH, pH 7.5, 140 mM NaCl, 1 mM EDTA, 10% glycerol, 0.5% Igepal, 0.25% Triton X-100, 1× complete protease inhibitor (Roche)]. The lysate was centrifuged at 800 ***g*** for 10 min and the cell pellet was resuspended and incubated for 10 min in 1 ml LB-B [10 mM Tris-HCl, pH 8.0, 200 mM NaCl, 1 mM EDTA, pH 8.0, 0.5 mM EGTA, pH 8.0, 1× complete protease inhibitor (Roche)]. The lysate was centrifuged at 800 ***g*** for 10 min and the nuclear pellet was resuspended and incubated for 10 min in 1 ml LB-C [50 mM Hepes, pH 7.5, 40 mM NaCl, 1 mM EDTA, 1 mM EGTA, 1% Triton X-100, 0.1% Na-deoxycholate, 0.1% SDS, pH 8.0, 1× complete protease inhibitor (Roche)]. Nuclear lysate was sonicated (seven times: 30 s, 4 cycles) with a Bioruptor (Diagenode). The sonicated sample was centrifuged at 18,000 ***g*** for 10 min and 50 µl of the supernatant was collected for input control. The rest of the supernatant (~950 µl) was rotated with 60 µl protein G Dynabeads (Invitrogen) for 3 h for pre-clearing. The beads were discarded and the pre-cleared lysate was rotated with 5 µg of anti-GFP (A11122, Invitrogen) antibody overnight. In parallel, 40 µl protein G Dynabeads were rotated with blocking buffers (0.5% BSA and 0.5% Tween-20 in PBS without Ca^{2+} and Mg^{2+}) overnight for pre-blocking. The next day, pre-cleared antibody-bound chromatin complexes (Ab-chromatin complexes) were rotated with pre-blocked beads for 1.5 h. The Ab-chromatin complex-bound beads were washed each time for 5 min with the following buffers: RIPA buffer [10 mM Tris-HCl, pH 8.0, 1 mM EDTA, pH 8.0, 140 mM NaCl, 1% Triton X-100, 0.1% SDS, 0.1% Na-deoxycholate, 1× complete protease inhibitor (Roche)]; five times with RIPA buffer without protease inhibitor; twice with RIPA-500 buffer (10 mM Tris-HCl, pH 8.0, 1 mM EDTA, pH 8.0, 500 mM NaCl, 1% Triton X-100, 0.1% Na-deoxycholate); twice with LiCl buffer (10 mM Tris-HCl, pH 8.0, 1 mM EDTA, pH 8.0, 250 mM LiCl, 0.5% NP-40, 0.5% Na-deoxycholate) and once with TE buffer (10 mM Tris-HCl, pH 8.0, 1 mM EDTA, pH 8.0). The beads were then resuspended in 50 µl elution buffer (10 mM Tris-HCl, pH 8.0, 5 mM EDTA, pH 8.0, 300 mM NaCl, 0.5% SDS) with 2 µg RNase A (Invitrogen) and incubated for 30 min at 37°C. Proteinase K (2.5 µl, 20 mg/ml; Invitrogen) was added and the reaction incubated overnight at 62°C for reverse cross-linking. The beads were then discarded. A DNA purification step, to extract chromatin fragments, was performed with solid phase reversible immobilisation (SPRI) beads using 2.3 volumes of SPRI beads per volume of sample for 4 min (Blecher-Gonen et al., 2013). Beads were then washed twice with 70% ethanol and air-dried for 4 min. Chromatin was eluted in 30 µl Tris buffer (10 mM). A size-selection step was performed with SPRI beads by first adding 0.6 volumes (18 µl) of SPRI beads per volume of sample and incubation for 4 min at room temperature. Beads binding chromatin fragments larger than 500 bp were then discarded. Subsequently, the chromatin was incubated with 1.8 volumes (36 µl) of SPRI beads for 4 min at room temperature, washed twice with 70% ethanol and air-dried for 4 min. Chromatin was eluted in 30 µl Tris buffer (10 mM).

qPCR was performed from 2 µl immunoprecipitated chromatin or 2 µl input sample, using a Rotorgene 6000 thermal cycler (Corbett Research), SYBR Green I (Molecular Probes) and Platinum Taq DNA Polymerase (Invitrogen). The following primers were used: *Dkk1* H1 region, 5′-CGAGGTTTGATTTGGGATCA-3′ and 5′-CACATGAGATCAAAG-TGGCT-3′; *Lhx1* +30R region, 5′-CCTGTGCTCTCTTGTCCAT-3′ and 5′-AGGCCTGACATTTCCAACAT-3′; *Lhx1* +1.5R region, 5′-AAACA-GACAGAAGGCGAGAT-3′ and 5′-TCCGTTTCGGCATCAAGGA-3′; *Lhx1* −6.5R region 5′-GCTTGTGGATGTCAGATACT-3′ and 5′-TCTG-GGGAACTTCAAACGTA-3′; NOBR region +8142-8341 bp upstream of *Dkk1* START codon, 5′-AAACTGGCTGCCCATCCAT-3′ and 5′-TCCC-GACAATACTAGGGATA-3′. PCR conditions (Fossat et al., 2011) were similar for all regions. The relative enrichment of a region in the immunoprecipitated sample was determined by normalising the C_t value obtained from the immunoprecipitated sample to the C_t value obtained from the input sample. Relative enrichment was calculated by the following equation: $2^{\text{input Ct–immunoprecipitated Ct}}$.

Bioinformatics

Mouse and human genomic sequence were analysed with the University of California, Santa Cruz (UCSC) genomic browser and YASS (Noe and Kucherov, 2005).

Acknowledgements

We thank Xin Wang for help with flow cytometry, performed in the Flow Cytometry Centre supported by the Westmead Millennium Institute, the NHMRC and the Cancer Institute, NSW, Australia. We thank the CMRI Bioservices Unit for animal care.

Competing interests

The authors declare no competing financial interests.

Author contributions

C.K.I., N.F. and V.J. performed the experiments, and T.L. provided the experimental materials. C.K.I., N.F. and P.P.L.T. designed the experiments, analysed the data and prepared the manuscript for publication.

Funding

This work was supported by the National Health and Medical Research Council (NHMRC) [Grant ID 632777] and by Mr James Fairfax. C.K.I. is a University of Sydney International Postgraduate Research Scholar and an Australian Postgraduate Awardee, N.F. is a Sir Norman Gregg Research Fellow of the Children's Medical Research Institute (CMRI) and P.P.L.T. is a NHMRC Senior Principal Research Fellow [Grant ID 1003100].

Supplementary material

Supplementary material available online at
http://dev.biologists.org/lookup/suppl/doi:10.1242/dev.114900/-/DC1

Development (2014) 141, 3859-3867 doi:10.1242/dev.114900

References

Acampora, D., Mazan, S., Lallemand, Y., Avantaggiato, V., Maury, M., Simeone, A. and Brulet, P. (1995). Forebrain and midbrain regions are deleted in Otx2-/- mutants due to a defective anterior neuroectoderm specification during gastrulation. *Development* **121**, 3279-3290.

Acampora, D., Avantaggiato, V., Tuorto, F., Briata, P., Corte, G. and Simeone, A. (1998). Visceral endoderm-restricted translation of Otx1 mediates recovery of Otx2 requirements for specification of anterior neural plate and normal gastrulation. *Development* **125**, 5091-5104.

Acampora, D., Boyl, P. P., Signore, M., Martinez-Barbera, J. P., Ilengo, C., Puelles, E., Annino, A., Reichert, H., Corte, G. and Simeone, A. (2001). OTD/OTX2 functional equivalence depends on 5′ and 3′ UTR-mediated control of Otx2 mRNA for nucleo-cytoplasmic export and epiblast-restricted translation. *Development* **128**, 4801-4813.

Acampora, D., Di Giovannantonio, L. G. and Simeone, A. (2013). Otx2 is an intrinsic determinant of the embryonic stem cell state and is required for transition to a stable epiblast stem cell condition. *Development* **140**, 43-55.

Ang, S. L., Conlon, R. A., Jin, O. and Rossant, J. (1994). Positive and negative signals from mesoderm regulate the expression of mouse Otx2 in ectoderm explants. *Development* **120**, 2979-2989.

Ang, S. L., Jin, O., Rhinn, M., Daigle, N., Stevenson, L. and Rossant, J. (1996). A targeted mouse Otx2 mutation leads to severe defects in gastrulation and formation of axial mesoderm and to deletion of rostral brain. *Development* **122**, 243-252.

Arkell, R. M. and Tam, P. P. (2012). Initiating head development in mouse embryos: integrating signalling and transcriptional activity. *Open Biol.* **2**, 120030.

Arkell, R. M., Fossat, N. and Tam, P. P. L. (2013). Wnt signalling in mouse gastrulation and anterior development: new players in the pathway and signal output. *Curr. Opin. Genet. Dev.* **23**, 454-460.

Blecher-Gonen, R., Barnett-Itzhaki, Z., Jaitin, D., Amann-Zalcenstein, D., Lara-Astiaso, D. and Amit, I. (2013). High-throughput chromatin immunoprecipitation for genome-wide mapping of in vivo protein-DNA interactions and epigenomic states. *Nat. Protoc.* **8**, 539-554.

Cajal, M., Lawson, K. A., Hill, B., Moreau, A., Rao, J., Ross, A., Collignon, J. and Camus, A. (2012). Clonal and molecular analysis of the prospective anterior neural boundary in the mouse embryo. *Development* **139**, 423-436.

Camus, A., Davidson, B. P., Billiards, S., Khoo, P., Rivera-Perez, J. A., Wakamiya, M., Behringer, R. R. and Tam, P. P. (2000). The morphogenetic role of midline mesendoderm and ectoderm in the development of the forebrain and the midbrain of the mouse embryo. *Development* **127**, 1799-1813.

Chatelain, G., Fossat, N., Brun, G. and Lamonerie, T. (2006). Molecular dissection reveals decreased activity and not dominant negative effect in human OTX2 mutants. *J. Mol. Med.* **84**, 604-615.

Downs, K. M. and Davies, T. (1993). Staging of gastrulating mouse embryos by morphological landmarks in the dissecting microscope. *Development* **118**, 1255-1266.

Fossat, N., Chatelain, G., Brun, G. and Lamonerie, T. (2006). Temporal and spatial delineation of mouse Otx2 functions by conditional self-knockout. *EMBO Rep.* **7**, 824-830.

Fossat, N., Le Greneur, C., Béby, F., Vincent, S., Godement, P., Chatelain, G. and Lamonerie, T. (2007). A new GFP-tagged line reveals unexpected Otx2 protein localization in retinal photoreceptors. *BMC Dev. Biol.* **7**, 122.

Fossat, N., Jones, V., Khoo, P.-L., Bogani, D., Hardy, A., Steiner, K., Mukhopadhyay, M., Westphal, H., Nolan, P. M., Arkell, R. et al. (2011). Stringent requirement of a proper level of canonical WNT signalling activity for head formation in mouse embryo. *Development* **138**, 667-676.

Fossat, N., Jones, V., Garcia-Garcia, M. J. and Tam, P. P. L. (2012). Modulation of WNT signaling activity is key to the formation of the embryonic head. *Cell Cycle* **11**, 26-32.

Fossat, N., Tourle, K., Radziewic, T., Barratt, K., Liebhold, D., Studdert, J. B., Power, M., Jones, V., Loebel, D. A. F. and Tam, P. P. L. (2014). C to U RNA editing mediated by APOBEC1 requires RNA-binding protein RBM47. *EMBO Rep.* **15**, 903-910.

Hallonet, M., Kaestner, K. H., Martin-Parras, L., Sasaki, H., Betz, U. A. K. and Ang, S.-L. (2002). Maintenance of the specification of the anterior definitive endoderm and forebrain depends on the axial mesendoderm: a study using HNF3beta/Foxa2 conditional mutants. *Dev. Biol.* **243**, 20-33.

Iwafuchi-Doi, M., Matsuda, K., Murakami, K., Niwa, H., Tesar, P. J., Aruga, J., Matsuo, I. and Kondoh, H. (2012). Transcriptional regulatory networks in epiblast cells and during anterior neural plate development as modeled in epiblast stem cells. *Development* **139**, 3926-3937.

Kemp, C., Willems, E., Abdo, S., Lambiv, L. and Leyns, L. (2005). Expression of all Wnt genes and their secreted antagonists during mouse blastocyst and postimplantation development. *Dev. Dyn.* **233**, 1064-1075.

Kimura, C., Yoshinaga, K., Tian, E., Suzuki, M., Aizawa, S. and Matsuo, I. (2000). Visceral endoderm mediates forebrain development by suppressing posteriorizing signals. *Dev. Biol.* **225**, 304-321.

Kimura, C., Shen, M. M., Takeda, N., Aizawa, S. and Matsuo, I. (2001). Complementary functions of Otx2 and Cripto in initial patterning of mouse epiblast. *Dev. Biol.* **235**, 12-32.

Kimura-Yoshida, C., Nakano, H., Okamura, D., Nakao, K., Yonemura, S., Belo, J. A., Aizawa, S., Matsui, Y. and Matsuo, I. (2005). Canonical Wnt signaling and its antagonist regulate anterior-posterior axis polarization by guiding cell migration in mouse visceral endoderm. *Dev. Cell* **9**, 639-650.

Kwan, K. M. and Behringer, R. R. (2002). Conditional inactivation of Lim1 function. *Genesis* **32**, 118-120.

Kwon, G. S., Viotti, M. and Hadjantonakis, A.-K. (2008). The endoderm of the mouse embryo arises by dynamic widespread intercalation of embryonic and extraembryonic lineages. *Dev. Cell* **15**, 509-520.

Lewis, S. L., Khoo, P.-L., Andrea De Young, R., Bildsoe, H., Wakamiya, M., Behringer, R. R., Mukhopadhyay, M., Westphal, H. and Tam, P. P. L. (2007). Genetic interaction of Gsc and Dkk1 in head morphogenesis of the mouse. *Mech. Dev.* **124**, 157-165.

Li, J. Y. and Joyner, A. L. (2001). Otx2 and Gbx2 are required for refinement and not induction of mid-hindbrain gene expression. *Development* **128**, 4979-4991.

Martinez-Barbera, J. P., Signore, M., Boyl, P. P., Puelles, E., Acampora, D., Gogoi, R., Schubert, F., Lumsden, A. and Simeone, A. (2001). Regionalisation of anterior neuroectoderm and its competence in responding to forebrain and midbrain inducing activities depend on mutual antagonism between OTX2 and GBX2. *Development* **128**, 4789-4800.

Matsuo, I., Kuratani, S., Kimura, C., Takeda, N. and Aizawa, S. (1995). Mouse Otx2 functions in the formation and patterning of rostral head. *Genes Dev.* **9**, 2646-2658.

Mukhopadhyay, M., Shtrom, S., Rodriguez-Esteban, C., Chen, L., Tsukui, T., Gomer, L., Dorward, D. W., Glinka, A., Grinberg, A., Huang, S. P. et al. (2001). Dickkopf1 is required for embryonic head induction and limb morphogenesis in the mouse. *Dev. Cell* **1**, 423-434.

Noe, L. and Kucherov, G. (2005). YASS: enhancing the sensitivity of DNA similarity search. *Nucleic Acids Res.* **33**, W540-W543.

Park, E. J., Sun, X., Nichol, P., Saijoh, Y., Martin, J. F. and Moon, A. M. (2008). System for tamoxifen-inducible expression of cre-recombinase from the Foxa2 locus in mice. *Dev. Dyn.* **237**, 447-453.

Perea-Gomez, A., Lawson, K. A., Rhinn, M., Zakin, L., Brulet, P., Mazan, S. and Ang, S. L. (2001). Otx2 is required for visceral endoderm movement and for the restriction of posterior signals in the epiblast of the mouse embryo. *Development* **128**, 753-765.

Pfister, S., Steiner, K. A. and Tam, P. P. L. (2007). Gene expression pattern and progression of embryogenesis in the immediate post-implantation period of mouse development. *Gene Expr. Patterns* **7**, 558-573.

Puelles, E., Acampora, D., Lacroix, E., Signore, M., Annino, A., Tuorto, F., Filosa, S., Corte, G., Wurst, W., Ang, S. L. et al. (2003). Otx dose-dependent integrated control of antero-posterior and dorso-ventral patterning of midbrain. *Nat. Neurosci.* **6**, 453-460.

Rhinn, M., Dierich, A., Shawlot, W., Behringer, R. R., Le Meur, M. and Ang, S. L. (1998). Sequential roles for Otx2 in visceral endoderm and neuroectoderm for forebrain and midbrain induction and specification. *Development* **125**, 845-856.

Rhinn, M., Dierich, A., Le Meur, M. and Ang, S. (1999). Cell autonomous and non-cell autonomous functions of Otx2 in patterning the rostral brain. *Development* **126**, 4295-4304.

Robb, L. and Tam, P. P. L. (2004). Gastrula organiser and embryonic patterning in the mouse. *Semin. Cell Dev. Biol.* **15**, 543-554.

Shawlot, W. and Behringer, R. R. (1995). Requirement for Lim1 in head-organizer function. *Nature* **374**, 425-430.

Shawlot, W., Wakamiya, M., Kwan, K. M., Kania, A., Jessell, T. M. and Behringer, R. R. (1999). Lim1 is required in both primitive streak-derived tissues and visceral endoderm for head formation in the mouse. *Development* **126**, 4925-4932.

Shimono, A. and Behringer, R. R. (1999). Isolation of novel cDNAs by subtractions between the anterior mesendoderm of single mouse gastrula stage embryos. *Dev. Biol.* **209**, 369-380.

Shimono, A. and Behringer, R. R. (2003). Angiomotin regulates visceral endoderm movements during mouse embryogenesis. *Curr. Biol.* **13**, 613-617.

Soriano, P. (1999). Generalized lacZ expression with the ROSA26 Cre reporter strain. *Nat. Genet.* **21**, 70-71.

Tam, P. P. (1989). Regionalisation of the mouse embryonic ectoderm: allocation of prospective ectodermal tissues during gastrulation. *Development* **107**, 55-67.

Tam, P. P. and Steiner, K. A. (1999). Anterior patterning by synergistic activity of the early gastrula organizer and the anterior germ layer tissues of the mouse embryo. *Development* **126**, 5171-5179.

Tanaka, S. S., Yamaguchi, Y. L., Steiner, K. A., Nakano, T., Nishinakamura, R., Kwan, K. M., Behringer, R. R. and Tam, P. P. L. (2010). Loss of Lhx1 activity impacts on the localization of primordial germ cells in the mouse. *Dev. Dyn.* **239**, 2851-2859.

Thomas, P. and Beddington, R. (1996). Anterior primitive endoderm may be responsible for patterning the anterior neural plate in the mouse embryo. *Curr. Biol.* **6**, 1487-1496.

Wang, J., Zhuang, J., Iyer, S., Lin, X., Whitfield, T. W., Greven, M. C., Pierce, B. G., Dong, X., Kundaje, A., Cheng, Y. et al. (2012). Sequence features and chromatin structure around the genomic regions bound by 119 human transcription factors. *Genome Res.* **22**, 1798-1812.

Zakin, L., Reversade, B., Virlon, B., Rusniok, C., Glaser, P., Elalouf, J.-M. and Brulet, P. (2000). Gene expression profiles in normal and Otx2-/- early gastrulating mouse embryos. *Proc. Natl. Acad. Sci. USA* **97**, 14388-14393.

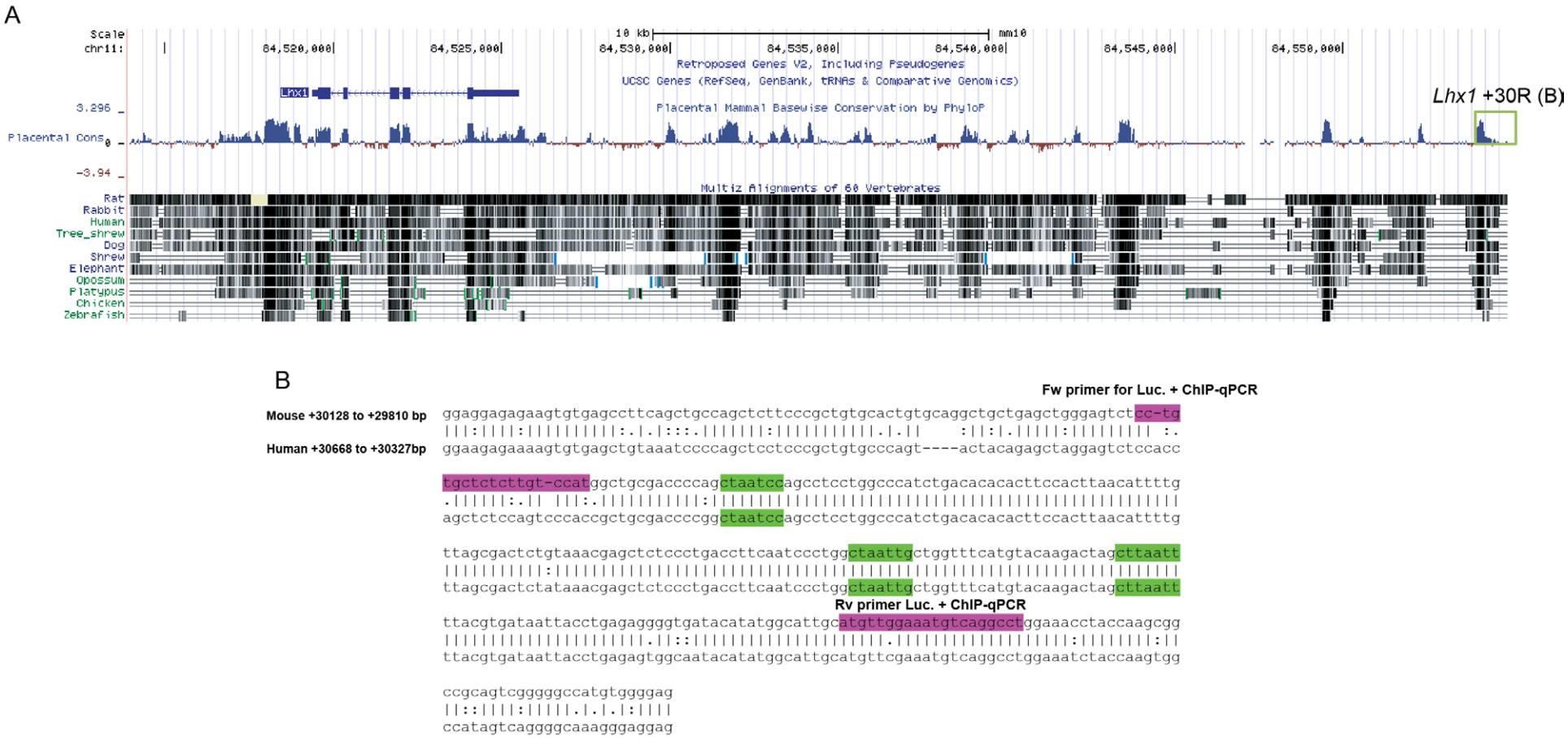

Supplementary Fig. S1. Mouse +30R region of *Lhx1*. (**A**) Genomic information of the *Lhx1* locus in mouse obtained from the University of California, Santa Cruz (UCSC) genomic browser. *Lhx1* is in antisens orientation. Thick blue boxes indicate coding sequences and thin blue boxes indicate untranslated regions. Placental mammal basewise conservation (Placental Cons) histogram shows the result of multiple sequence alignment for 60 vertebrate species. The conservation score was measured by phyloP. The blue bar indicates positive score in which the regions are conserved, whereas regions with negative score in red indicate are not conserved. Gray scale density plot display pairwise alignments for each species (Rat, Rabbit, Human, Tree_shrew, Dog, Shrew, Elephant, Opossum, Platypus, Chicken and Zebrafish). Gray scales with darker values indicate higher level of overall conservation scored by phastCons. The green box delineates the conserved genomic location covering the *Lhx1* +30R region. (**B**) Basewise sequence alignment of the mouse (+30128 to +29810 bp upstream of START codon) and the human (+30668 to +30327 bp upstream of START codon) +30R regions. Sequences of the primers used for ChIP-qPCR and luciferase (Luc.) assay are highlighted in purple. Fw, forward primer; Rv, reverse primer. Sequences highlighted in green refer to OTX2 binding motifs or motifs close to an OTX2 binding motif.

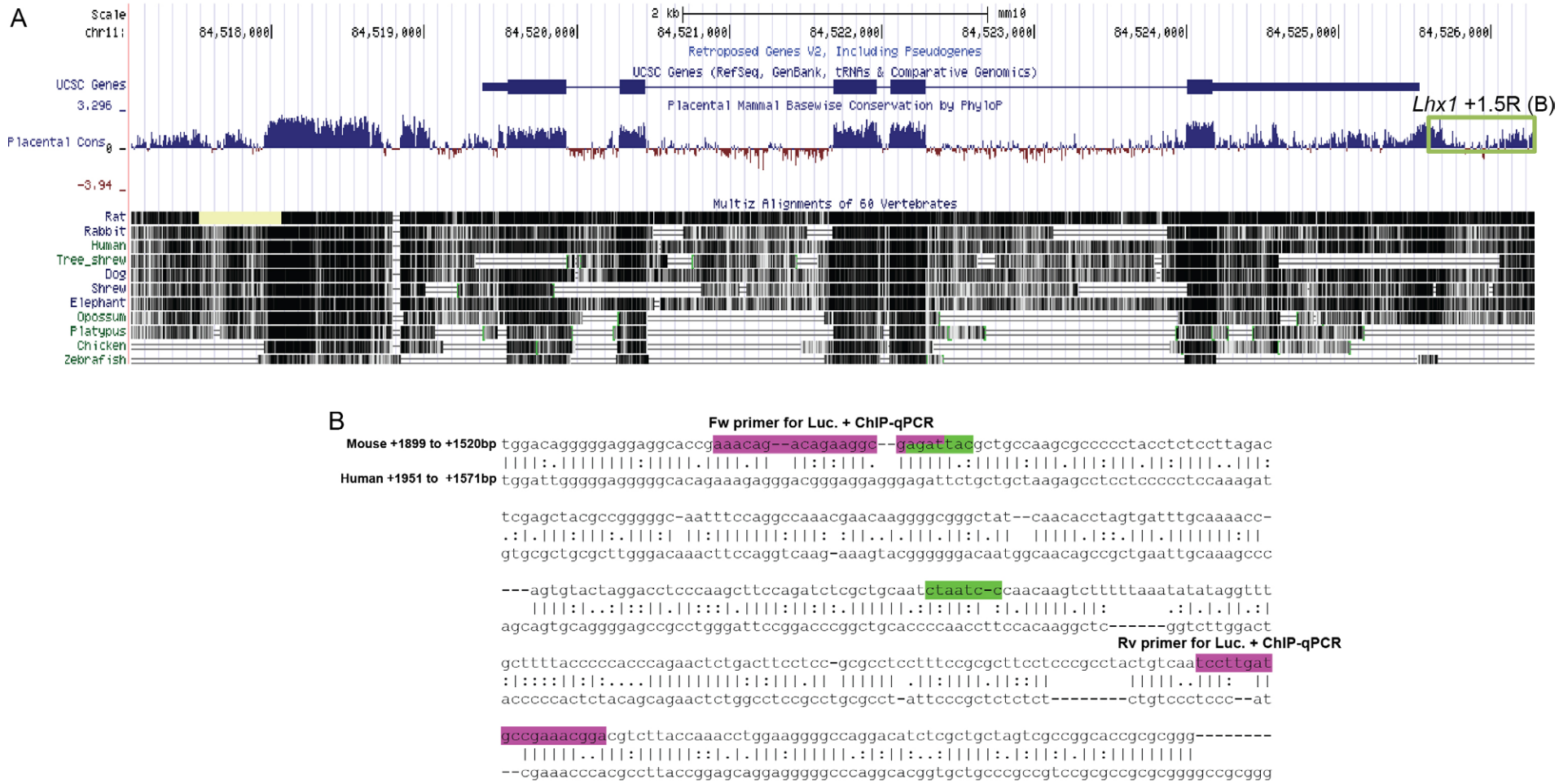

Supplementary Fig. S2. Mouse +1.5R region of *Lhx1*. (**A**) Genomic information of the *Lhx1* locus in mouse obtained from the University of California, Santa Cruz (UCSC) genomic browser. *Lhx1* is in antisens orientation. Thick blue boxes indicate coding sequences and thin blue boxes indicate untranslated regions. Placental mammal basewise conservation (Placental Cons) histogram shows the result of multiple sequence alignment for 60 vertebrate species. The conservation score was measured by phyloP. The blue bar indicates positive score in which the regions are conserved, whereas regions with negative score in red indicate are not conserved. Gray scale density plot display pairwise alignments for each species (Rat, Rabbit, Human, Tree_shrew, Dog, Shrew, Elephant, Opossum, Platypus, Chicken and Zebrafish). Gray scales with darker values indicate higher level of overall conservation scored by phastCons. The green box delineates the conserved genomic location covering the *Lhx1* +1.5R region. (**B**) Basewise sequence alignment of the mouse (+1899 to +1520 bp upstream of START codon) and the human (+1951 to +1571 bp upstream of START codon) +1.5R regions. Sequences of the primers used for ChIP-qPCR and luciferase (Luc.) assay are highlighted in purple. Fw, forward primer; Rv, reverse primer. Sequences highlighted in green refer to OTX2 binding motifs or motifs close to an OTX2 binding motif.

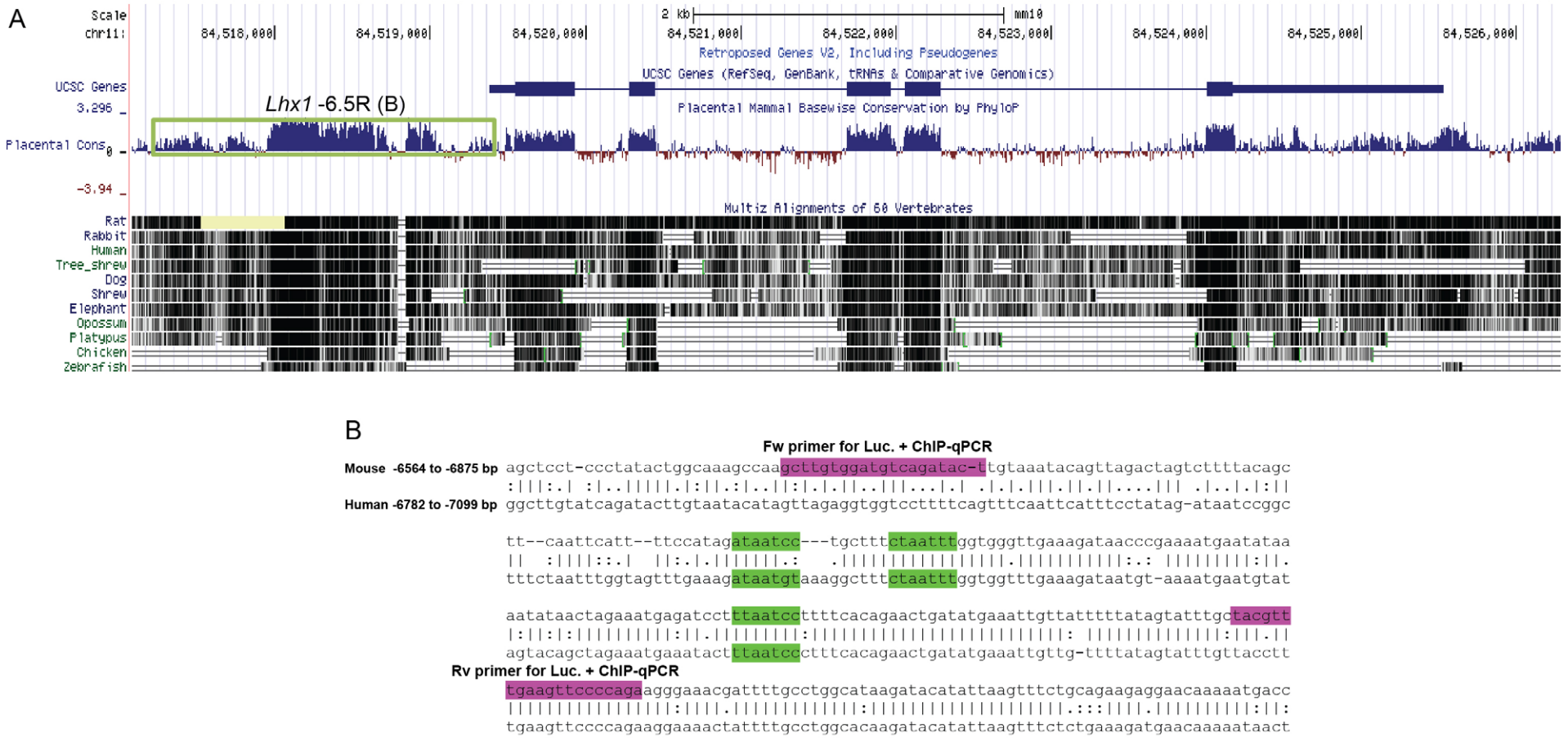

Supplementary Fig. S3. Mouse -6.5R region of *Lhx1*. (**A**) Genomic information of the *Lhx1* locus in mouse obtained from the University of California, Santa Cruz (UCSC) genomic browser. *Lhx1* is in antisens orientation. Thick blue boxes indicate coding sequences and thin blue boxes indicate untranslated regions. Placental mammal basewise conservation (Placental Cons) histogram shows the result of multiple sequence alignment for 60 vertebrate species. The conservation score was measured by phyloP. The blue bar indicates positive score in which the regions are conserved, whereas regions with negative score in red indicate are not conserved. Gray scale density plot display pairwise alignments for each species (Rat, Rabbit, Human, Tree_shrew, Dog, Shrew, Elephant, Opossum, Platypus, Chicken and Zebrafish). Gray scales with darker values indicate higher level of overall conservation scored by phastCons. The green box delineates the conserved genomic location covering the *Lhx1* -6.5R region. (**B**) Basewise sequence alignment of the mouse (-6564 to -6875 bp downstream of START codon) and the human (-6782 to -7099 bp downstream of START codon) -6.5R regions. Sequences of the primers used for ChIP-qPCR and luciferase (Luc.) assay are highlighted in purple. Fw, forward primer; Rv, reverse primer. Sequences highlighted in green refer to OTX2 binding motifs or motifs close to an OTX2 binding motif.